Calculation of Long-Range Interactions in Molecular Dynamics and Monte Carlo Simulations

Xuedong Din and Efstathios E. Michaelides*

School of Engineering, Tulane University, New Orleans, Louisiana 70118

Received: December 18, 1996; In Final Form: April 7, 1997[⊗]

The general expansion method is developed to calculate long-range interactions due to charged particles outside the minimum images, for different periodic systems in molecular dynamics and Monte Carlo simulations. The expansion coefficients are obtained by the least-squares method. The neighbor-box technique is also developed to calculate long- and short-range interactions within the minimum images. The interactions between neighbor particles are directly calculated, while the interactions between nonneighbor particles are obtained by interpolation. The combination of the general expansion (GE) method and the neighbor-box (NB) technique, named as the GENB method, renders the computation of long-range interactions proportional to $N^{3/2}$, where N is the total number of particles in the central cell. Most importantly, the GENB method can be easily used to study different periodic systems. As an example, water molecules in a cylindrical pore are simulated to demonstrate the computational efficiency and accuracy of the neighbor-box technique under different conditions.

1. Introduction

A major obstacle in molecular dynamics (MD) and Monte Carlo (MC) simulations is the excessive amount of CPU time. An important contributor to this is the calculation of the electrostatic force between charged particles, which is a long-range interaction. Since this interaction varies slowly with the distance between particles, several hundred replicas of the central cell in each periodic dimension are needed in order to obtain convergent results.

A number of different methods have been used to take long-range interactions into account. The Ewald summation method is widely used for computing the electrostatic energy due to an infinite array of point-charge images in periodic systems.[1−7] Transformation algorithms[8] have also been developed to speed up the computations of the summations, and improved algorithms of the order $n(\log n)$ using fast Fourier transforms have been reported.[9,10] The reaction field method[11−15] assumes that the surrounding medium beyond a cutoff distance is a dielectric continuum, and the field produced at the center of the truncation sphere, by the polarization of the medium outside the sphere, is the Onsager reaction field. In the expansion methods, the lattice sums of the long-range interactions in periodic systems may be expressed in terms of Bessel functions[16] or by multipoles.[17,18] Recently, efficient algorithms based on multipole expansion techniques have been developed.[19]

Despite the large amount of work in the past years, several problems concerning the calculation of long-range interactions for the above methods still remain unsolved. For example, the Ewald summation method was originally developed for a cubic central cell extended periodically in three dimensions. Therefore, for periodic systems constrained by walls, the Ewald summation method is not valid. The reaction field method is not strictly consistent with the periodicity of the system, and the existence of boundary walls also introduces difficulties in calculating the reaction field. The expansion methods have been used to study periodic systems between plates.[16] However, it is still necessary to develop more efficient algorithms for the cells of complex shapes.

The aim of this paper is to present a new algorithm in order to calculate the long-range interactions in different periodic systems. We first develop a general expansion method to calculate the electrostatic energy and the potentials in the central cell, due to the contributions of particles outside the minimum images. Then the neighbor-box technique is introduced and used to calculate the short-range interactions and to interpolate the long-range interactions to every particle in the central cell. The combination of the general expansion (GE) method and the neighbor-box (NB) technique renders the computational complexity of long-range interactions proportional to $N^{3/2}$, where N is the total number of particles in the central cell. In the final section we use the GENB method to simulate water molecules in a cylindrical pore.

2. The General Expansion Method

2.1. Energy and Potentials in Periodic Systems. We consider a central cell of N particles with charges q_i ($i = 1, N$) under periodic conditions. The computer simulation is carried out in a box of dimensions D_x, D_y, and D_z in the x, y, and z directions, respectively. The characteristic length of the central cell, D, will be defined later for different systems. It is convenient to introduce a dimensionless geometric parameter λ as follows:

$$\lambda = \max\left(\frac{D_x}{D}, \frac{D_y}{D}, \frac{D_z}{D}\right) \tag{1}$$

Three kinds of periodic systems are often used in simulations:

(a) One periodic dimension (1PD): The central cell is replicated infinitely in the z direction and the other dimensions are constrained by walls. We define the characteristic length D as $D \equiv D_z$. If D_z is larger than D_x and D_y, then $\lambda = 1$; otherwise, $\lambda > 1$. In this study we will consider systems with $\lambda \leq 2$.

(b) Two periodic dimensions (2PD): The central cell is replicated infinitely in the y and z directions, while the sides in the x direction are constrained by walls. We assume $D_y = D_z = D$. If D is larger than D_x, then $\lambda = 1$; otherwise, $\lambda > 1$. In this study we will consider systems with $\lambda \leq 2$.

* Author to whom correspondence should be addressed.

[⊗] Abstract published in *Advance ACS Abstracts,* May 15, 1997.

S1089-5639(97)00030-3 CCC: $14.00

(c) Three periodic dimensions (3PD): The central cell is replicated infinitely in all the three dimensions. This is an unconfined system. In this case the central cell is a cube, i.e., $D \equiv D_x = D_y = D_z$, and $\lambda = 1$.

The dimensionless distances between two points $\mathbf{r}_i = (x_i,y_i,z_i)$ and $\mathbf{r}_j = (x_j,y_j,z_j)$ in the central cell are defined as

$$\xi = \frac{x_i - x_j}{D}, \quad \eta = \frac{y_i - y_j}{D}, \quad \zeta = \frac{z_i - z_j}{D}, \quad d^2 = \xi^2 + \eta^2 + \zeta^2 \tag{2}$$

We express the electrostatic energy of the central cell in a general form for the three periodic systems as follows:

$$E = \frac{1}{2}\sum_{i=1}^{N}\sum_{j=1}^{N} q_i q_j \sum_{|'\mathbf{n}|=0}^{\infty} \frac{1}{|\mathbf{r}_i - \mathbf{r}_j + D\mathbf{n}|} = \frac{1}{2}\sum_{i=1}^{N}\sum_{j=1}^{N} q_i q_j \phi(\mathbf{r}_i,\mathbf{r}_j) \tag{3}$$

where $\phi(\mathbf{r}_i,\mathbf{r}_j)$ is the electrostatic potential at point $\mathbf{r}_i$ due to a unit charge at $\mathbf{r}_j$ and all of its images. The prime symbol indicates that the term for which $|\mathbf{r}_i - \mathbf{r}_j + D\mathbf{n}| = 0$ is neglected. The sum over $\mathbf{n}$ is a sum over the lattice vectors. For 3PD, $\mathbf{n} = l\mathbf{i}_x + m\mathbf{i}_y + n\mathbf{i}_z$, where $(\mathbf{i}_x,\mathbf{i}_y,\mathbf{i}_z)$ are the unit vectors in the three dimensions and (l,m,n) are integers; for 2PD, $\mathbf{n} = m\mathbf{i}_y + n\mathbf{i}_z$; and for 1PD, $\mathbf{n} = n\mathbf{i}_z$. The central cell corresponds to $\mathbf{n} = 0$, and the minimum images consist of these replicas satisfying $|\mathbf{n}| \le 1$. Hence, the minimum images of 1PD, 2PD, and 3PD have 3, 9, and 27 replicas, respectively. The summations in $\phi(\mathbf{r}_i,\mathbf{r}_j)$ may be separated into two parts: the first one is the contributions of the particles in the minimum images, and the second part includes the interactions of particles in other replicas:

$$\phi(\mathbf{r}_i,\mathbf{r}_j) = \frac{1}{D}\Psi(\mathbf{r}_i,\mathbf{r}_j) + \sum_{|n|\le 1}^{1} \frac{1}{|\mathbf{r}_i - \mathbf{r}_j + D\mathbf{n}|} \tag{4}$$

where $\Psi(\mathbf{r}_i,\mathbf{r}_j)$ is a dimensionless quantity due to the contributions of particles outside the minimum images. For 3PD, this quantity is

$$\Psi(\mathbf{r}_i,\mathbf{r}_j) = \sum_{l=\infty}^{\infty}{}'' \sum_{m=\infty}^{\infty}{}'' \sum_{n=\infty}^{\infty}{}'' \frac{1}{(l^2 + m^2 + n^2)^{1/2}(1+\beta)^{1/2}} \tag{5}$$

with

$$\beta = \frac{2\xi l + 2\eta m + 2\zeta n + d^2}{l^2 + m^2 + n^2} \tag{6}$$

The double primes indicate summations which exclude the minimum images. We can express $\phi(\mathbf{r}_i,\mathbf{r}_j)$ for 1PD and 2PD in a similar way. If the summation for l is dropped out (i.e., $l \equiv 0$) from eqs 5 and 6, we obtain $\phi(\mathbf{r}_i,\mathbf{r}_j)$ and β for 2PD; and if the summations for l and m are dropped out (i.e., $l = m \equiv 0$) from eqs 5 and 6, we obtain $\phi(\mathbf{r}_i,\mathbf{r}_j)$ and β for 1PD. For the three periodic systems considered here, we obtain the ranges of β as follows: for 1PD and $\lambda \le 2$, $-0.75 \le \beta \le 3.25$; for 2PD and $\lambda \le 2$, $-0.75 \le \beta \le 1.75$; and for 3PD and $\lambda = 1$, $-0.75 \le \beta \le 1.25$.

The total energy of the system may be expressed in the following form:

$$E = \frac{1}{2}\sum_{i=1}^{N}\sum_{j=1}^{N} q_i q_j \left[\frac{1}{D}\Psi(\mathbf{r}_i,\mathbf{r}_j) + \sum_{|n|\le 1} \frac{1}{|\mathbf{r}_i - \mathbf{r}_j + D\mathbf{n}|}\right] \tag{7}$$

Although eq 5 is divergent, we will show in section 2.2 that the divergent term does not matter in the calculation of the electrostatic force. Because the electrostatic potential varies slowly with distance, the summations in eq 5 must be carried out for at least several hundreds replicas in each periodic dimension. Therefore, it is not realistic for any practical computer simulations to directly use eq 5 to calculate $\Psi(\mathbf{r}_i,\mathbf{r}_j)$. For this reason we use the expansion method in order to facilitate the calculation. This method fields the summations indicated in eq 5 independently of the particles' relative positions ξ, η, and ζ.

2.2. Finite Expansion Method. The function $(1+\beta)^{-1/2}$ is expressed as a power series of ξ, η, and ζ, and then the variables are taken out of the summation operations. The function $(1+\beta)^{-1/2}$ may be expanded as a Taylor series or Legendre polynomials. These methods have two major limitations: First, the absolute value of β must be less than 1 for convergence. Second, many terms are needed in order to keep the truncation errors small. The function $(1+\beta)^{-1/2}$ can be replicated by a series of polynomials of β. For the three periodic systems considered here, β varies in the range $-0.75 \le \beta \le 3.25$. Hence, we consider the following eighth-order approximation:

$$\frac{1}{(1+\beta)^{1/2}} \approx e_0 + e_1\beta + e_2\beta^2 + e_3\beta^3 + e_4\beta^4 + e_5\beta^5 + e_6\beta^6 + e_7\beta^7 + e_8\beta^8 \tag{8}$$

where the constants e_i ($i = 0, 8$) are chosen in such a way that (for the range of interest) the values of $(1+\beta)^{-1/2}$ can be best fitted by the right-hand side of eq 8. Using the least-squares method we obtain the following coefficients:

e_0, 1.0023844; e_1, −0.4728575; e_2, 0.3087774;
e_3, −0.3916828; e_4, 0.5303276; e_5, −0.4061865;
e_6, 0.1637860; e_7, $-0.3299228 \times 10^{-1}$;
e_8, 0.2623945×10^{-2}

The relative error of this eq is less than 0.8% in the range $-0.76 \le \beta \le 3.34$.

From eq 6 the powers of β can be further expanded in terms of ξ, η, and ζ. After substituting eq 8 into eq 5, the summations for l, m, and n can be accomplished independent of the variables ξ, η, and ζ. The odd powers of l, m, and n cancel out, due to symmetry. We must emphasize that, in this procedure the first term e_0 in eq 8 corresponds to a series, which is divergent as the summations for l, m, and n are carried out to infinity. If the central cell satisfies the charge neutrality condition, the contributions of the positive and negative charges cancel each other. Therefore, this term may be ignored. On the other hand, if there is a net charge in the system, the potential due to this term corresponds to a large constant, which tends to infinity as the summations for l, m, and n are carried out to infinity. In this case the term e_0 introduces a large uniform background potential. Again we may ignore this uniform potential without affecting the dynamic properties of the system, because only the differences of the potential affect the motion of particles. It must be pointed out that, because the system considered is periodic, and because the periodicity is intrinsic in the calculations, the removal of the background potential does not render the system a nonconducting one. Therefore, after neglecting the divergent term e_0, the expansion formulas are still valid to net-charge systems. In the latter case, the potential to be considered is the relative potential, that is, the difference between the real potential and the uniform background potential.

For convenience we define the following summation conventions:

(a) for 1PD:

$$K^i = \sum_{n=\infty}^{\infty}{}'' \frac{1}{|n|^i} \tag{9}$$

(b) for 2PD:

$$M^i N^j K^k = \sum_{m=\infty}^{\infty}{}'' \sum_{n=\infty}^{\infty}{}'' \frac{m^i n^j}{(m^2+n^2)^{i+j+k/2}} \tag{10}$$

(c) for 3PD:

$$L^i M^j N^k K^t = \sum_{l=\infty}^{\infty}{}'' \sum_{m=\infty}^{\infty}{}'' \sum_{n=\infty}^{\infty}{}'' \frac{l^i m^j n^k}{(l^2+m^2+n^2)^{i+j+k+t/2}} \tag{11}$$

These constants are directly obtained from numerical computations and are given in Tables 1, 2, and 3. For the 3PD case, if K^3 and L^2K are transformed into integrations, they are conditionally convergent, but not absolutely convergent.[3] In the present work, although the numerical summations for these two constants converge very slowly, it seems that they approach the steady values as the lattice numbers used in the summations increase. In Table 3 the values of K^3 and L^2K are obtained by using 8000 replicas in each dimension.

TABLE 1: K^i for 1PD

$K^3 = 0.404114$	$K^5 = 0.738555 \times 10^{-1}$	$K^7 = 0.166986 \times 10^{-1}$
$K^9 = 0.401679 \times 10^{-2}$	$K^{11} = 0.988377 \times 10^{-3}$	$K^{13} = 0.245427 \times 10^{-3}$
$K^{15} = 0.611765 \times 10^{-4}$	$K^{17} = 0.152744 \times 10^{-4}$	

The final result is to express the function $\Psi(\mathbf{r}_i,\mathbf{r}_j)$ in the following polynomial forms:

(a) for 1PD:

$$\begin{aligned}\Psi(\mathbf{r}_i,\mathbf{r}_j) = {} & (e_1 d^2 + 4e_2\,\zeta^2)K^3 + (e_2 d^4 + 12e_3 d^2\,\zeta^2 + \\ & 16e_4\,\zeta^4)K^5 + (e_3 d^6 + 24e_4 d^4\,\zeta^2 + 80e_5 d^2\,\zeta^4 + 64e_6\,\zeta^6)K^7 + \\ & (e_4 d^8 + 40e_5 d^6\,\zeta^2 + 240e_6 d^4\,\zeta^4 + 448e_7 d^2\,\zeta^6 + \\ & 256e_8\,\zeta^8)K^9 + (e_5 d^{10} + 60e_6 d^8\,\zeta^2 + 560e_7 d^6\,\zeta^4 + \\ & 1792e_8 d^4\,\zeta^6)K^{11} + (e_6 d^{12} + 84e_7 d^{10}\,\zeta^2 + \\ & 1120e_8 d^8\,\zeta^4)K^{13} + (e_7 d^{14} + 112e_8 d^{12}\,\zeta^2)K^{15} + e_8 d^{16} K^{17}\end{aligned} \tag{12}$$

(b) for 2PD:

$$\begin{aligned}\Psi(\mathbf{r}_i,\mathbf{r}_j) = {} & e_1 K^3 d^2 + 4e_2 M^2 K(\eta^2+\zeta^2) + e_2 K^5 d^4 + \\ & 12e_3 M^2 K^3(\eta^2+\zeta^2)d^2 + 16e_4 M^4 K(\eta^4+\zeta^4) + \\ & 96e_4 M^2 N^2 K\,\eta^2\,\zeta^2 + e_3 K^7 d^6 + 24e_4 M^2 K^5(\eta^2+\zeta^2)d^4 + \\ & 80e_5 M^4 K^3(\eta^4+\zeta^4)d^2 + 480e_5 M^2 N^2 K^3\,\eta^2\,\zeta^2\,d^2 + \\ & 64e_6 M^6 K(\eta^6+\zeta^6) + 960e_6 M^4 N^2 K(\eta^2+\zeta^2)\,\eta^2\,\zeta^2 + \\ & e_4 K^9 d^8 + 40e_5\, M^2 K^7(\eta^2+\zeta^2)d^6 + 240e_6 M^4 K^5(\eta^4 + \\ & \zeta^4)d^4 + 1440e_6 M^2 N^2 K^5\,\eta^2\,\zeta^2 d^4 + 448e_7 M^6 K^3(\eta^6+\zeta^6)d^2 + \\ & 6720e_7 M^4 N^2 K^3(\eta^2+\zeta^2)\,\eta^2\,\zeta^2\,d^2 + 256e_8 M^8 K(\eta^8+\zeta^8) + \\ & 7168e_8 M^6 N^2 K(\eta^4+\zeta^4)\,\eta^2\,\zeta^2 + 17920e_8 M^4 N^4 K\,\eta^4\,\zeta^4 + \\ & e_5 K^{11} d^{10} + 60e_6 M^2 K^9(\eta^2+\zeta^2)d^8 + 560e_7 M^4 K^7(\eta^4 + \\ & \zeta^4)d^6 + 3360e_7 M^2 N^2 K^7\,\eta^2\,\zeta^2\,d^6 + 1792e_8 M^6 K^5(\eta^6 + \\ & \zeta^6)d^4 + 26880e_8 M^4 N^2 K^5(\eta^2+\zeta^2)\,\eta^2\,\zeta^2\,d^4 + e_6 K^{13} d^{12} + \\ & 84e_7 M^2 K^{11}(\eta^2+\zeta^2)d^{10} + 1120e_8 M^4 K^9(\eta^4+\zeta^4)d^8 + \\ & 6720e_8 M^2 N^2 K^9\,\eta^2\,\zeta^2\,d^8 + e_7 K^{15} d^{14} + 112e_8 M^2 K^{13}(\eta^2 + \\ & \zeta^2)d^{12} + e_8 K^{17} d^{16}\end{aligned} \tag{13}$$

TABLE 2: $M^iN^jK^k$ For 2PD

$K^3 = 0.361870 \times 10$	$M^2K = 0.180935 \times 10$	$K^5 = 0.383151$
$M^2K^3 = 0.191576$	$M^4K = 0.153803$	$M^2N^2K = 0.377724 \times 10^{-1}$
$K^7 = 0.695644 \times 10^{-1}$	$M^2K^5 = 0.347822 \times 10^{-1}$	$M^4K^3 = 0.289059 \times 10^{-1}$
$M^2N^2K^3 = 0.587627 \times 10^{-2}$	$M^6K = 0.259678 \times 10^{-1}$	$M^4N^2K = 0.293813 \times 10^{-2}$
$K^9 = 0.144917 \times 10^{-1}$	$M^2K^7 = 0.724583 \times 10^{-2}$	$M^4K^5 = 0.619693 \times 10^{-2}$
$M^2N^2K^5 = 0.104890 \times 10^{-2}$	$M^6K^3 = 0.567248 \times 10^{-2}$	$M^4N^2K^3 = 0.524452 \times 10^{-3}$
$M^8K = 0.532304 \times 10^{-2}$	$M^6N^2K = 0.349438 \times 10^{-3}$	$M^4N^4K = 0.175014 \times 10^{-3}$
$K^{11} = 0.319897 \times 10^{-2}$	$M^2K^9 = 0.159948 \times 10^{-2}$	$M^4K^7 = 0.140160 \times 10^{-2}$
$M^2N^2K^7 = 0.197878 \times 10^{-3}$	$M^6K^5 = 0.130267 \times 10^{-2}$	$M^4N^2K^5 = 0.989390 \times 10^{-4}$
$K^{13} = 0.728364 \times 10^{-3}$	$M^2K^{11} = 0.364182 \times 10^{-3}$	$M^4K^9 = 0.325854 \times 10^{-3}$
$M^2N^2K^9 = 0.383284 \times 10^{-4}$	$K^{15} = 0.169119 \times 10^{-3}$	$M^2K^{13} = 0.845593 \times 10^{-4}$
$K^{17} = 0.398205 \times 10^{-4}$		

TABLE 3: $L^iM^jN^kK^t$ For 3PD

$K^3 = 0.986843 \times 10^2$	$L^2K = 0.328948 \times 10^2$	$K^5 = 0.174299 \times 10$
$L^2K^3 = 0.580997$	$L^2M^2K = 0.102809$	$L^4K = 0.375379$
$K^7 = 0.235331$	$L^2K^5 = 0.784436 \times 10^{-1}$	$L^2M^2K^3 = 0.122344 \times 10^{-1}$
$L^4M^2K = 0.544126 \times 10^{-2}$	$L^4K^3 = 0.539749 \times 10^{-1}$	$L^6K = 0.430923 \times 10^{-1}$
$L^2M^2N^2K = 0.135187 \times 10^{-2}$	$K^9 = 0.415069 \times 10^{-1}$	$L^2K^7 = 0.138356 \times 10^{-1}$
$L^2M^2K^5 = 0.189294 \times 10^{-2}$	$L^4M^2K^3 = 0.854536 \times 10^{-3}$	$L^6M^2K = 0.525465 \times 10^{-3}$
$L^4K^5 = 0.100497 \times 10^{-1}$	$L^6K^3 = 0.834066 \times 10^{-2}$	$L^2M^2N^2K^3 = 0.183872 \times 10^{-3}$
$L^4M^2N^2K = 0.612907 \times 10^{-4}$	$L^8K = 0.728973 \times 10^{-2}$	$L^4M^4K = 0.267781 \times 10^{-3}$
$K^{11} = 0.812204 \times 10^{-2}$	$L^2K^9 = 0.270735 \times 10^{-2}$	$L^2M^2K^7 = 0.322907 \times 10^{-3}$
$L^4M^2K^5 = 0.147694 \times 10^{-3}$	$L^4K^7 = 0.206153 \times 10^{-2}$	$L^6K^5 = 0.176615 \times 10^{-2}$
$L^2M^2N^2K^5 = 0.275193 \times 10^{-4}$	$K^{13} = 0.168125 \times 10^{-2}$	$L^2K^{11} = 0.560418 \times 10^{-3}$
$L^2M^2K^9 = 0.578203 \times 10^{-4}$	$L^4K^9 = 0.444777 \times 10^{-3}$	$K^{15} = 0.361099 \times 10^{-3}$
$L^2K^{13} = 0.120366 \times 10^{-3}$	$K^{17} = 0.797076 \times 10^{-4}$	

(c) for 3P*D*:

$$\Psi(\mathbf{r}_i,\mathbf{r}_j) = (e_1K^3 + 4e_2L^2K)d^2 + (e_2K^5 + 12e_3L^2K^3 + 48e_4L^2M^2K)d^4 + 16e_4(L^4K - 3L^2M^2K)\,(\xi^4 + \eta^4 + \zeta^4) + (e_3K^7 + 24e_4L^2K^5 + 240e_5L^2M^2K^3 + 320e_6L^4M^2K)d^6 + 80e_5(L^4K^3 - 3L^2M^2K^3)\,(\xi^4 + \eta^4 + \zeta^4)d^2 + 64e_6(L^6K - 5L^4M^2K)\,(\xi^6 + \eta^6 + \zeta^6) + 1920e_6(3L^2M^2N^2K - L^4M^2K)\,\xi^2\,\eta^2\,\zeta^2 + (e_4K^9 + 40e_5L^2K^7 + 720e_6L^2M^2K^5 + 2240e_7L^4M^2K^3 + 1792e_8L^6M^2K)d^8 + 240e_6(L^4K^5 - 3L^2M^2K^5)\,(\xi^4 + \eta^4 + \zeta^4)d^4 + 448e_7(L^6K^3 - 5L^4M^2K^3)\,(\xi^6 + \eta^6 + \zeta^6)d^2 + (40320L^2M^2N^2K^3e_7 - 13440L^4M^2K^3e_7 + 107520L^4M^2N^2Ke_8 - 21504L^6M^2Ke_8)\,\xi^2\,\eta^2\,\zeta^2\,d^2 + 256e_8(L^8K - 7L^6M^2K)(\xi^8 + \eta^8 + \zeta^8) + 256e_8(70L^4M^4K - 42L^6M^2K)(\xi^4\,\eta^4 + \xi^4\,\zeta^4 + \eta^4\,\zeta^4) + (e_5K^{11} + 60e_6L^2K^9 + 1680e_7L^2M^2K^7 + 8960e_8L^4M^2K^5)d^{10} + 560e_7(L^4K^7 - 3L^2M^2K^7)\,(\xi^4 + \eta^4 + \zeta^4)d^6 + 1792e_8(L^6K^5 - 5L^4M^2K^5)\,(\xi^6 + \eta^6 + \zeta^6)d^4 + 1792e_8(90L^2M^2N^2K^5 - 30L^4M^2K^5)\,\xi^2\,\eta^2\,\zeta^2\,d^4 + (e_6K^{13} + 84e_7L^2K^{11} + 3360e_8L^2M^2K^9)d^{12} + 1120e_8(L^4K^9 - 3L^2M^2K^9)\,(\xi^4 + \eta^4 + \zeta^4)d^8 + (e_7K^{15} + 112e_8L^2K^{13})d^{14} + e_8K^{17}d^{16} \quad (14)$$

In order to test the accuracy of these formulae we consider a central cell with only two counter-ions as depicted in Figure 1. Particle 1 is always located at the origin ($\mathbf{r}_1 = 0$), while particle 2 may be anywhere in the box. Without loss of generality, we assume $D = 1$ and $-q_1 = q_2 = 1$. The central cell is divided into mesh points with starting point at (0.05, 0.05, 0.05) and a uniform increment of 0.1 in the three dimensions. We locate particle 2 at the following mesh points, respectively:

(a) For 1PD: Noting the symmetry between *x* and *y* directions in eq 12, for the central cell with $\lambda \le 2$, we locate particle 2 at the mesh points which satisfy $0 < x \le y < 2$, and $0 < z < 1$. The total number of the points is 2100.

(b) For 2PD: Noting the symmetry between *y* and *z* directions in eq 13, for the central cell with $\lambda \le 2$, we locate particle 2 at the mesh points which satisfy $0 < x < 2$, and $0 < y \le z < 1$. The total number of the points is 1100.

(c) For 3PD: Noting the symmetry between *x*, *y*, and *z* directions in eq 14, for the central cell with $\lambda = 1$, we locate particle 2 at the mesh points satisfying $0 < x \le y \le z < 1$. The total number of the points is 220.

For the different positions of particle 2, the exact values of the electrostatic energy in the central cell can be directly calculated from eq 3 over enough replicas in each periodic dimension. In this study, the number of the replicas used in each dimension is 2000 for 1PD and 2PD, and 500 for 3PD. The electrostatic energy may also be obtained from eqs 7, 12, 13, and 14 for different periodic systems. Table 4 lists the maximum errors of eqs 12−14 at the mesh points, and the total energy errors of all the points. Here the total energy of each system is the summation of the energy, when particle 2 is located at different mesh points. The relative errors of these formulas are rather high and exceed the value of 0.8%, the error limit of eq 8 when $-0.76 \le \beta \le 3.34$. The decrease of accuracy is probably caused by the fact that the leading term of eq 8 has been canceled. However, eqs 12−14 are still useful, because they demonstrate the forms of the expansion formulas for $\Psi(\mathbf{r}_i,\mathbf{r}_j)$. We follow these forms and develop more accurate formulas for Q in the following section.

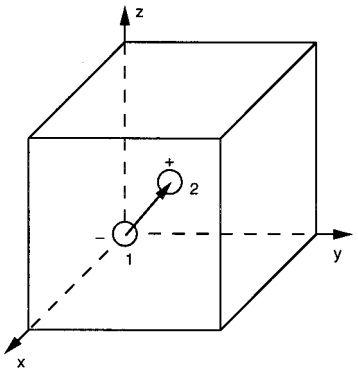

Figure 1. Cell with two counterions.

TABLE 4: Energy Errors of Eqs 12, 13, and 14 at the Mesh Points

	absolute error	relative error (%)	total energy error (%)
eq 12 for 1PD	2.1×10^{-2}	115	1.6
eq 13 for 2PD	0.27	206	3.8
eq 14 for 3PD	0.60	466	4.3

2.3. General Expansion Method. In the previous section we have used an eighth order polynomial to approximate the function $(1 + \beta)^{-1/2}$. However, the accuracy of the final formulas for $\Psi(\mathbf{r}_i,\mathbf{r}_j)$ is worse than the expansion eq 8. If the function $(1 + \beta)^{-1/2}$ is approximated more closely by keeping more terms in the expansion, the higher order terms of β will make the expansion formulas very complex. An alternative method is the general expansion method, which has been developed to overcome this accuracy problem. Following eqs 12−14, we observe that any expansion series of β will result in the following general forms for $\Psi(\mathbf{r}_i,\mathbf{r}_j)$:

(a) for 1PD:

$$\Psi(\mathbf{r}_i,\mathbf{r}_j) = (e_{11} + e_{12}d^2 + e_{13}d^4 + e_{14}d^6 + e_{15}d^8 + ...)d^2 + (e_{21} + e_{22}d^2 + e_{23}d^4 + e_{24}d^6 + e_{25}d^8 + ...)\zeta^2 + (e_{31} + e_{32}d^2 + e_{33}d^4 + e_{34}d^6 + e_{35}d^8 + ...)\zeta^4 + (e_{41} + e_{42}d^2 + e_{43}d^4 + e_{44}d^6 + e_{45}d^8 + ...)\zeta^6 + (e_{51} + e_{52}d^2 + e_{53}d^4 + e_{54}d^6 + e_{55}d^8 + ...)\zeta^8 + ... \quad (15)$$

(b) for 2PD:

$$\Psi(\mathbf{r}_i,\mathbf{r}_j) = (e_{11} + e_{12}d^2 + e_{13}d^4 + e_{14}d^6 + e_{15}d^8 + ...)d^2 + (e_{21} + e_{22}d^2 + e_{23}d^4 + e_{24}d^6 + e_{25}d^8 + ...)\,(\eta^2 + \zeta^2) + (e_{31} + e_{32}d^2 + e_{33}d^4 + e_{34}d^6 + e_{35}d^8 + ...)\,(\eta^4 + \zeta^4) + (e_{41} + e_{42}d^2 + e_{43}d^4 + e_{44}d^6 + e_{45}d^8 + ...)\,(\eta^6 + \zeta^6) + (e_{51} + e_{52}d^2 + e_{53}d^4 + e_{54}d^6 + e_{55}d^8 + ...)\,(\eta^8 + \zeta^8) + (e_{61} + e_{62}d^2 + e_{63}d^4 + e_{64}d^6 + e_{65}d^8 + ...)\eta^2\zeta^2 + (e_{71} + e_{72}d^2 + e_{73}d^4 + e_{74}d^6 + e_{75}d^8 + ...)\eta^4\zeta^4 + (e_{81} + e_{82}d^2 + e_{83}d^4 + e_{84}d^6 + e_{85}d^8 + ...)\,(\eta^2 + \zeta^2)\eta^2\zeta^2 + (e_{91} + e_{92}d^2 + e_{93}d^4 + e_{94}d^6 + e_{95}d^8 + ...)\,(\eta^2 + \zeta^2)\eta^4\zeta^4 + ... \quad (16)$$

(c) for 3PD:

$$\Psi(\mathbf{r}_i,\mathbf{r}_j) = (e_{11} + e_{12}d^2 + e_{13}d^4 + e_{14}d^6 + e_{15}d^8 + ...)d^2 + (e_{21} + e_{22}d^2 + e_{23}d^4 + e_{24}d^6 + e_{25}d^8 + ...)(\xi^4 + \eta^4 + \zeta^4) + (e_{31} + e_{32}d^2 + e_{33}d^4 + e_{34}d^6 + e_{35}d^8 + ...)(\xi^6 + \eta^6 + \zeta^6) + (e_{41} + e_{42}d^2 + e_{43}d^4 + e_{44}d^6 + e_{45}d^8 + ...)(\xi^8 + \eta^8 + \zeta^8) + (e_{51} + e_{52}d^2 + e_{53}d^4 + e_{54}d^6 + e_{55}d^8 + ...)\xi^2\eta^2\zeta^2 + (e_{61} + e_{62}d^2 + e_{63}d^4 + e_{64}d^6 + e_{65}d^8 + ...)(\xi^4\eta^4 + \xi^4\zeta^4 + \eta^4\zeta^4) + ... \quad (17)$$

where e_{ij} are constants for each periodic system. Instead of following the method of section 2.2, we evaluate these constants by optimization in such a way that the energy calculated by eqs 15−17 can best fit the exact values at the mesh points in the cell of Figure 1. Using the least-squares method, we obtain the constants in Tables 5−7. These constants are generally valid for systems containing many particles, because the interactions between two particles are determined only by their relative positions.

Table 8 summarizes the energy errors calculated from the above formulas with the above coefficients. A comparison between Tables 4 and 8 shows that the accuracy of these formulas has been dramatically improved at every mesh point. Furthermore, the total energy errors of the systems remain very small. Calculations at other nonmesh points also reveal that these equations manifest the same order of accuracy. This implies that eqs 15−17 represent correctly the variations of $\Psi(\mathbf{r}_i,\mathbf{r}_j)$ in the periodic systems. Because far more mesh points have been used for 1PD and 2PD than for 3PD, eqs 15 and 16 have larger errors than eq 17. However, eqs 15 and 16 are valid over a wider range of conditions ($\lambda \leq 2$).

We have also tried to include more coefficients in eqs 15 and 16 in order to increase the accuracy. However, the improvement achieved by including more terms is not significant. It must be pointed out that if we only consider smaller systems ($\lambda \leq 1.5$), the same number of constants as in Tables 5 and 6 can make eqs 15 and 16 reach very high accuracy. In this case, the constants are different from those in Tables 5 and 6 and should be determined by the least-squares method for a smaller λ. Considering that in practical simulations statistical errors due to limited simulation time are of the order of 3%, we believe that the eqs 15 to 17 with the constants in Tables 5−7 are adequate and may be applied to most practical simulations.

It must be pointed out that in some practical applications involving slabs or cylinders, there are image forces arising between charges and the wall. These forces depend on the dielectric properties of the wall and play an important role in the determination of the behavior of the charges next to the wall. This paper presents a mathematical model for the calculation of the long-range forces and does not explicitly account for these image forces. However, if one knows the particular form of the image forces and if these forces are long-range forces, then the same mathematical technique and the same formulas can be used with relative ease for the calculation of all the interactions, including image forces, between wall particles and other charges in the periodic systems under consideration.

Regarding the dielectric behavior of the systems studied, in the strictly periodic three-dimensional system, the images extend to infinity in all three dimensions. Because of this, one does not need to make any assumptions about the dielectric behavior of the surroundings. The dielectric behavior of the system may then be directly obtained from the MD simulations. In the case of the one- and two-dimensional systems, one does not need to make any assumptions about the surroundings in the periodic directions. However, one needs to make an assumption about the way of interaction between the wall and the other charges in the (nonperiodic) directions constrained by the walls. For example, one may prescribe a certain charge distribution at the wall particles and then use the GENB method, as described above, to investigate how the dielectric behavior of the system will be affected by the prescribed distribution of charges.

3. Neighbor-Box Technique

3.1. Interpolation Scheme. If we calculate the energy of the system directly from eq 7 and the general expansion

TABLE 5: e_{ij} for 1PD and $\lambda \leq 2$ (Other $e_{ij} = 0$)

	$j=1$	$j=2$	$j=3$	$j=4$	$j=5$
$i=1$	−0.2077424E+00	0.3428627E−01	−0.7106388E−02	0.9221446E−03	−0.4758371E−04
$i=2$	0.6525880E+00	−0.3325861E+00	0.1061282E+00	−0.1659468E−01	0.9557752E−03
$i=3$	0.9311387E−01	0.1294186E+00	−0.1014672E+00	0.2175868E−01	−0.1449539E−02
$i=4$	0.4547276E+00	−0.6302982E+00	0.2784920E+00	−0.4824246E−01	0.2844989E−02
$i=5$	−0.7632409E−01	0.2246102E+00	−0.1210333E+00	0.2276231E−01	−0.1396308E−02

TABLE 6: e_{ij} for 2PD and $\lambda \leq 2$ (Other $e_{ij} = 0$)

$j=1$	$j=2$	$j=3$	$j=4$	$j=5$	
$i=1$	−0.1816724E+01	−0.1699775E+00	−0.4174220E−01	−0.9328132E−02	−0.9021478E−03
$i=2$	−0.2735749E+01	−0.8144851E+00	−0.2867662E+00	−0.6810108E−01	−0.6941093E−02
$i=3$	−0.6560462E+00	−0.3418037E+00	−0.1039581E+00	−0.1847906E−01	−0.9708847E−03
$i=4$	−0.3093328E+00	−0.6165123E+00	−0.3198507E+00	−0.6095910E−01	−0.3863707E−02
$i=5$	−0.3261200E+00	−0.1267820E+00	−0.1961777E−01	−0.1235827E−01	−0.1161693E−02
$i=6$	−0.9631366E+00	−0.3292370E+00	−0.3165100E−01	−0.1012508E−01	−0.3040349E−02
$i=7$	−0.1008012E+01	−0.4574110E+00	−0.6432559E−01	−0.7212198E−02	−0.7874020E−03
$i=8$	−0.5285276E+00	−0.1029238E+01	−0.4744796E+00	−0.7867250E−01	−0.4695472E−02
$i=9$	−0.4604183E+00	−0.1477914E+00	−0.2303130E+00	−0.5850997E−01	−0.4454742E−02

TABLE 7: e_{ij} for 3PD and $\lambda = 1$ (Other $e_{ij} = 0$)

	$j=1$	$j=2$	$j=3$	$j=4$	$j=5$
$i=1$	−0.1624441E−03	−0.1840786E+00	−0.1360559E+00	−0.2026793E+00	−0.1069545E−01
$i=2$	−0.3119160E+00	−0.3209188E+00	−0.6623410E−01	−0.1626264E+00	−0.2577575E−01
$i=3$	−0.1181618E+00	−0.1265090E+01	−0.8145192E+00	−0.3992228E+00	−0.6944240E−01
$i=4$	−0.1140781E+01	−0.7393993E+00	−0.3010605E+00	−0.1284144E−01	−0.1827551E−01
$i=5$	−0.7151641E+00	−0.2737381E+01	−0.1160333E+00	−0.7387805E−01	−0.2794727E−01
$i=6$	−0.1494817E+01	−0.2071101E+00	−0.1467369E+00	−0.7977268E−01	−0.6923794E−02

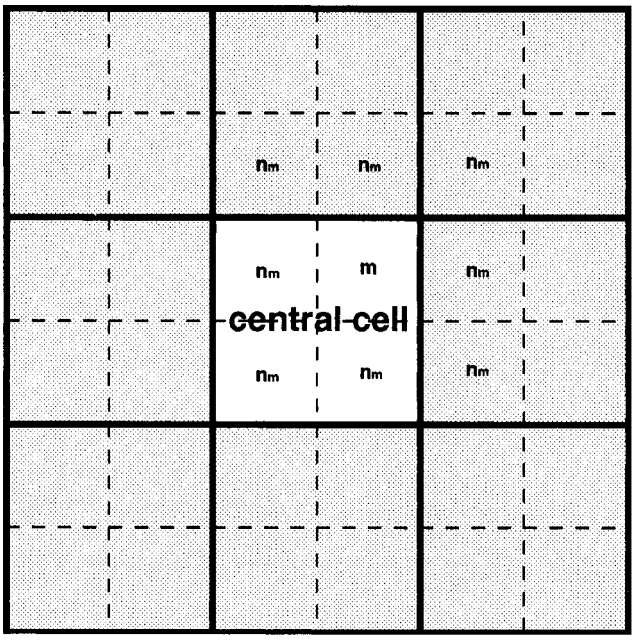

Figure 2. Central cell and the minimum images divided into smaller boxes. To the box m in the central cell, those boxes indicated by n_m are its neighbor boxes.

TABLE 8: Energy Errors of Eqs 15, 16, and 17 at the Mesh Points

	absolute error	relative error (%)	total energy error (%)
eq 15 for 1PD	1.6×10^{-2}	3.2	4.8×10^{-3}
eq 16 for 2PD	6.2×10^{-3}	3.0	1.5×10^{-4}
eq 17 for 3PD	5.0×10^{-4}	0.98	5.3×10^{-5}

equations, the total number of operations will be proportional to N^2, where N is the total number of particles in the central cell. Since the computational complexity of N^2 is an obstacle for large systems, it is necessary to develop more efficient algorithms to calculate the energy of the system.

For the case of short-range interactions we have developed the neighbor-box technique in order to improve the computational efficiency. The basic premise of this technique is that the minimum images are subdivided into many boxes, as shown in Figure 2. The sides of each box are longer than the highest cutoff radius of all the short-ranged interactions. The neighbor boxes of a given box are these, which have at least one common point with the given box. Those boxes, which are outside the central cell but are located inside the minimum images, should also be taken into account in the neighbor boxes. The particles in the same box or its neighbor boxes are called neighbor particles. To calculate the forces on a particle in the given box, we only take into account the interactions between this particle and the neighbor particles. The essence of this method is similar to the link-cell method.[20]

We modify and extend the neighbor-box method to the computation of long-range interactions. The basis of the calculations is that for a particle in the given box, the long-range interactions between this particle and the neighbor particles are calculated directly, while the interactions between this particle and particles outside the neighbor boxes are obtained by interpolation. There is an intrinsic assumption in this method that the interactions between neighbor particles may vary sharply with distance, while the interactions between nonneighbor particles will change slowly with distance.

We assume that the total box number in the central cell is M. For a given box, m, in the central cell, the number of the neighbor particles is N_m, and the number of the nonneighbor particles within the minimum images is $\overline{N_m}$. For 1PD, $\overline{N_m} = 3NN_m$; for 2PD, $\overline{N_m} = 9NN_m$; and for 3PD, $\overline{N_m} = 27NN_m$. Noting that $|\mathbf{n}| \leq 1$ corresponds to the particles within the minimum images, we may express eq 7 as

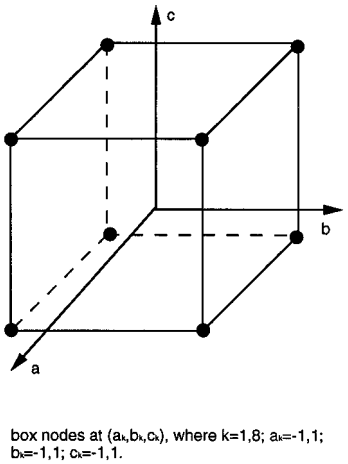

Figure 3. The 8-node box (trilinear element).

$$E = E_1 + E_2 \tag{18}$$

with

$$E_1 = \frac{1}{2}\sum_{i=1}^{N}\sum_{j\in N_m}\frac{q_i q_j}{|\mathbf{r}_i\mathbf{r}_j|}, \quad E_2 = \frac{1}{2}\sum_{i=1}^{N} q_i \Phi(r_i) \tag{19}$$

and

$$\Phi(\mathbf{r}_i) = \sum_{j=1}^{N}\frac{q_j}{D}\Psi(\mathbf{r}_i\mathbf{r}_j) + \sum_{j\in\overline{N_m}}\frac{q_j}{|\mathbf{r}_i\mathbf{r}_j|} \tag{20}$$

where the particle i is located in the box m, and $\in$ indicates that the particle j belongs to N_m or $\overline{N_m}$.

In MD simulations, we have to calculate the electrostatic forces on a particle, i.e., $\mathbf{F}_i = -\nabla_i E$, where ∇_i means the gradient with respect to $\mathbf{r}_i$. In this case, we have

$$\mathbf{F}_i = \mathbf{F}_i^{\,1} + \mathbf{F}_i^{\,2} \tag{21}$$

with

$$\mathbf{F}_i^{\,1} = -q_i\sum_{j'\in N_m}\Delta_i\left(\frac{q_j}{|\mathbf{r}_i,\mathbf{r}_j|}\right), \quad \mathbf{F}_i^{\,2} = -q_i\Delta_i\Phi(\mathbf{r}_i) \tag{22}$$

Because the minimum images are divided into many small boxes, N_m is generally much smaller than $\overline{N_m}$. Therefore, in the computation of the energy and the forces, the total number of operations is mainly determined by the calculation of E_2 and $\mathbf{F}_i^2$. In this study, the interpolation method is used to reduce the computation of these terms.

Two kinds of boxes are considered: one is the trilinear element with 8 nodes and the other is the complete quadratic element with 27 nodes, which are depicted in Figures 3 and 4. The first is widely used in the finite element method.[21, 22] We first calculate the value of Φ at those nodes of the box, i.e., $\Phi(\mathbf{r}_{\text{node}})$. Then for every particle in the box, $\Phi(\mathbf{r}_i)$ and $\nabla_i\Phi(\mathbf{r}_i)$ are obtained by interpolation from the nodes at the particle position $\mathbf{r}_i$. Because the node number of a box is in general much less than the particle number in the box, the total number of operations in a given box can be substantially reduced.

We first consider the interpolation functions on the two line elements of Figure 5. The potentials are known at $a_1 = -1$

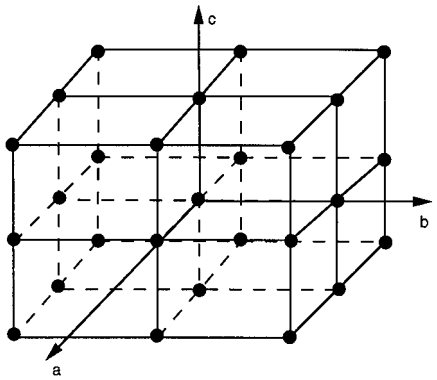

Figure 4. The 27-node box (complete quadratic element).

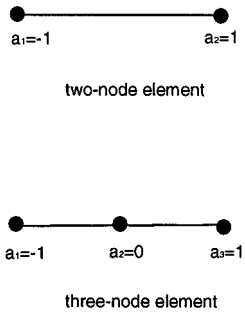

Figure 5. Line elements.

and $a_2 = 1$ for the 2-node element, or at $a_1 = -1$, $a_2 = 0$, and $a_3 = 1$ for the three-node element. For any point, a, in the elements, the potential may be approximated by an interpolation from the known nodes:

$$\Phi(a) = \sum_{k=1}^{n} h(a,a_k)\Phi(a_k) \qquad (1 \le a \le 1) \tag{23}$$

where n is equal to 2 for the 2-node element and 3 for the 3-node element, $\Phi(a_k)$ is the potential at the kth node, and $h(a,a_k)$ is an interpolation function which is similar to the one used in the finite element method:[22]

for the 2-node element:

$$h(a,a_k) = 0.5(1 + a_k a) \tag{24}$$

and for the 3-node element:

$$h(a,a_k) = 0.5[1S_k + a_k a + (1.5 - 0.5S_k)S_k a^2] \tag{25}$$

where $S_k = -1$ if $a_k = 0$; otherwise, $S_k = 1$.

The interpolation accuracy is of first order for the 2-node element and of second order for the 3-node element. The above two expressions can be used to construct the interpolation functions for the 8-node box and the 27-node box: Let the central cell be uniformly divided into M_x, M_y, and M_z segments in the x, y, and z directions, respectively. Then the number of boxes in the central cell is $M = M_x M_y M_z$, and the three sides of each box are $L_x = D_x/M_x$, $L_y = D_y/M_y$, and $L_z = D_z/M_z$, where L_x, L_y, and L_z must be longer than the highest cutoff radius of all the short-range interactions. For any point (x,y,z) in the box with center at (x_0,y_0,z_0), it is convenient to introduce the local coordinates:

$$a = \frac{2(x - x_0)}{L_x}, \quad \frac{2(y - y_0)}{L_y}, \quad \frac{2(z - z_0)}{L_z} \tag{26}$$

Obviously, $-1 \le a,b,c \le 1$. The potential at the kth node of the box, $\Phi(\mathbf{r}_{\text{node\_}k})$, is directly calculated from eq 20, where $\mathbf{r}_{\text{node\_}k}$ is the location of the kth node of the box in space. Then the potential at (a,b,c) is found by interpolation:[21]

$$\Phi(a,b,c) = \sum_{k=1}^{n} h(a,a_k)h(b,b_k)h(c,c_k)\Phi(\boldsymbol{r}_{\text{node\_}k}) \tag{27}$$

where n is 8 for the 8-node box and 27 for the 27-node box, (a_k,b_k,c_k) is the node position shown in Figures 3 and 4, h corresponds to eq 24 for the 8-node box and eq 25 for the 27-node box. The gradient of the potential is expressed as follows:

$$\frac{\partial\Phi}{\partial x} = \frac{2}{L_x}\sum_{k=1}^{n}\frac{\partial h(a,a_k)}{\partial a}h(b,b_k)h(c,c_k)\Phi(\boldsymbol{r}_{\text{node\_}k}) \tag{28}$$

$$\frac{\partial\Phi}{\partial y} = \frac{2}{L_y}\sum_{k=1}^{n}\frac{\partial h(b,b_k)}{\partial b}h(a,a_k)h(c,c_k)\Phi(\boldsymbol{r}_{\text{node\_}k}) \tag{29}$$

$$\frac{\partial\Phi}{\partial z} = \frac{2}{L_z}\sum_{k=1}^{n}\frac{\partial h(c,c_k)}{\partial c}h(a,a_k)h(b,b_k)\Phi(\boldsymbol{r}_{\text{node\_}k}) \tag{30}$$

We can use eqs 27−30 to calculate $\Phi(\mathbf{r}_i)$ and $\nabla_i\Phi(\mathbf{r}_i)$ on every particle in the central cell. Then, the energy of the system and the forces on every particle are calculated from eqs 18 and 21.

The accuracy of the interpolations is mainly determined by the node numbers and the box sizes. Generally, the 27-node box generates a higher accuracy, while the computational speed of the 8-node box is faster. In this scheme, the interactions between neighbor particles are directly calculated and only the interactions of nonneighbor particles are obtained by interpolation. Therefore, with the same node numbers, the larger the box the more accurate is the interpolation. This is different from the traditional finite element theory, where smaller elements lead to higher accuracy.

3.2. The GENB Method. The combined general expansion and neighbor-box method (GENB) for the calculation of the energy and forces, which includes both the short-range and long-range interactions on every particle in the central cell, may be implemented as follows:

Step 1: Divide the minimum images into many boxes, the sides of each box being larger than the highest cutoff radius of all the short-range interactions. Then determine the neighbor boxes of each box.

Step 2: For every particle in a given box, calculate the short-range interactions and the electrostatic interactions between this particle and other particles within this box and the neighbor boxes. Hence, obtain E_1 from eq 19 and $\mathbf{F}_i^1$ from eq 22.

Step 3: Calculate $\Phi(\mathbf{r}_{\text{node\_}k})$ at the nodes of each box from eq 20. Use eqs 15−17 for the different periodic systems.

Step 4: For every particle in a given box, interpolate $\Phi(\mathbf{r}_{\text{node\_}k})$ to the particle position to obtain $\Phi(\mathbf{r}_i)$ by eq 27, or calculate the gradient of $\Phi(\mathbf{r}_i)$ by eqs 28−30. Then obtain E_2 by eq 19 and $\mathbf{F}_i^2$ by eq 22. Thus, calculate the energy of the system and the forces on every particle.

An estimation on the operations of the above steps is as follows. We assume that the minimum images of the system is g_1, and the average number of the neighbor boxes is g_2. Then the operations from steps 2 to 4 are proportional to $N\overline{N_m}$, $nM(N + \overline{N_m})$, and nN. Generally, $N_m \approx g_2 N/M$, and $\overline{N_m} \approx g_1 N -$

g_2N/M. Consequently, the total number of operations, T, is approximately

$$T = c_1 g_2 \frac{N^2}{M} + c_2 nM\left(N + g_1 N g_2 \frac{N}{M}\right) + c_3 nN \qquad (31)$$

where the coefficients c_1, c_2, and c_3 are determined by the practical programming methods. When $M = [c_1 g_2 N/c_2 n(1 + g_1)]^{1/2}$, the operations reach the minimum value, which is $T = [4c_1 c_2 n g_2(1 + g_1)]^{1/2} N^{3/2} + (c_3 - c_2 g_2)nN$. That is, if M is properly selected, the total number of operations is proportional to $N^{3/2}$. We have to point out that, although the $O(n \log n)$ algorithms using fast Fourier transformations[9,10] are more efficient for 3PD, the GENB method can be easily used to study different periodic systems.

4. Simulation of Water Molecules in a Cylindrical Pore

Many computer studies on the equilibrium statistical properties of water molecules near walls have been reported in the past decade.[23−30] These investigations include water molecules on hydrophobic and hydrophilic walls, and ionic solutions. In order to study the computational efficiency and accuracy of the neighbor-box technique, we use the GENB method to simulate water molecules in a cylindrical carbon pore. This study may also be used to calculate statistical properties of a solvent in a fine capillary, an important problem of biological and industrial membranes.

The wall of the pore consists of 10 rings, each having 17 equally spaced carbon atoms on a circle of radius $R_w = 12.244$ Å. The rings are placed in a way that atoms form a triangular lattice on the cylinder surface. The diameter of the wall atoms is $\sigma_w = 3.2$ Å and the height of the cylinder is 22.627 Å. We use 200 water molecules in the simulation, where the water−water potential is determined by the SPC/E model.[31] We assume that the effective radius of the pore is 3.024 Å narrower than R_w. The value 3.024 is obtained from the zero-potential point of a structureless carbon plane.[27] Such a system corresponds to a bulk density of 1 g/cm^3. The interactions between water and carbon atoms are given by the Lennard-Jones potentials and the required parameters are chosen as $\sigma_{WO} = 3.183$ Å, $\sigma_{WH} = 2.942$ Å, $\epsilon_{WO} = 0.125$ kcal/mol, and $\epsilon_{WH} = 0.0772$ kcal/mol. The temperature of the system is kept at 29.5 °C by the Nosé−Hoover isothermal dynamics.[32] The SHAKE procedure[33] is used to maintain the internal geometry of the SPC/E molecules. A cutoff radius of 7.5 Å is used for all short-range interactions. The Verlet algorithm[34] is used with time step 2 fs. The initial state is obtained by using the 27-node box under $(M_x,M_y,M_z) = (2,2,2)$ to run 100 000 steps from a random configuration. We choose five configurations of water molecules as the reference states. This corresponds to the configurations obtained by running another $(n - 1)100$ steps from the initial state, where the integer n varies from 1 to 5. All the simulations in the present work were carried out in an IBM RISC/6000 workstation.

Table 9 shows the computational time and accuracy with different box numbers and box nodes. For the reference states mentioned above, the exact values of the forces on every water molecule are calculated without using the neighbor-box technique, in order to compare the accuracy of different interpolation schemes at the same instant. The average force on every water molecule is about 8.11g/F in the five reference states. In Table 9 the absolute error is the maximum value in the five reference states. The relative error is defined as the ratio of the absolute error to the average force on every molecule. With the same box division (M_x,M_y,M_z), the 27-node box is more accurate than the 8-node box. It is apparent that the most accurate scheme is the 27-node box under the divisions (1,1,1) and (2,2,1), which has a relative error less than 0.5%. The 8-node box under the divisions (1,1,1) and (2,2,1) also has reasonable error limits (<2.5%). If the box numbers in the constraint directions are less than 3, in most regions the electrostatic interactions between the molecules are directly calculated without interpolation errors by the GENB method. Therefore, the central cell can be divided by half in the constraint directions, without affecting the accuracy significantly. The 27-node box under the division (2,2,2) may also be used for practical simulations if simulation time is the main constraint. Since the interpolation error is more sensitive to the box size in the periodic direction, the box size in this direction should not be much smaller than the constraint sides.

TABLE 9: Force Errors on Molecules at the Reference States and the Relative Time To Run 100 Steps for Different Schemes[a]

nodes	(M_x,M_y,M_z)	absolute error (γ/σ)	relative error (%)	relative time
8	(1,1,1)	0.20	2.5	0.61
8	(2,2,2)	1.79	22	0.36
8	(3,3,3)	2.12	26	0.34
8	(1,1,2)	1.93	23	0.35
8	(2,2,1)	0.19	2.3	0.61
8	(3,3,1)	2.11	26	0.52
27	(1,1,1)	0.03	0.4	0.65
27	(2,2,2)	0.37	4.6	0.47
27	(3,3,3)	0.92	11	0.88
27	(1,1,2)	0.76	10	0.40
27	(2,2,1)	0.04	0.5	0.67
27	(3,3,1)	1.87	23	0.81

[a] The unit of time is the CPU time to run 100 steps without using the neighbor-box technique.

In Table 9 the CPU time to run 100 steps without using the neighbor-box technique is used as the unit of time. Then the CPU time of the other schemes to run 100 steps is compared with this time. We note that the neighbor-box technique demonstrates a substantial time reduction in all the cases considered. Under the same condition, the 8-node box is generally faster than the 27-node box as expected. The fastest speed is reached by the 8-node box with $(M_x,M_y,M_z) = (3,3,3)$. However, the error introduced under some conditions is unacceptable. For this problem, we recommend the 27-node box with $(M_x,M_y,M_z) = (1,1,1)$, (2,2,1), or (2,2,2).

It is evident that when a particle traverses through a cell side and finds itself into another cell, there is a discontinuity in the calculated values of energy and force. We considered the magnitude of this discontinuity and found out that it is of the same order as the magnitude of the errors listed in Table 8. This occurs because Table 8 lists the maximum energy error on every particle over different configurations of the system. In these configurations several particles have definitely traversed through the side of their cell into one of the neighboring cells. The discontinuity/error is caused mainly by the interpolation scheme in the neighbor-box technique and its order of magnitude remains the same when a particle traverses through a cell.

We have used the 27-node box with $(M_x,M_y,M_z) = (2,2,2)$ to simulate water molecules over 500 000 steps from the initial state. The density distributions of oxygen and hydrogen atoms are shown in Figure 6, where $\rho_O(r)$ and $\rho_H(r)$ are normalized by the number density of bulk water and the dotted lines correspond to the bulk values. We note that the density oscillations of the oxygen and hydrogen atoms are not so pronounced as the distribution of a simple fluid (like argon) near the wall. In the work of Zhu and Robinson[27] the hydrogen density at the first peak near a neutral wall is larger than the bulk value, while Figure 6 shows that this number is smaller

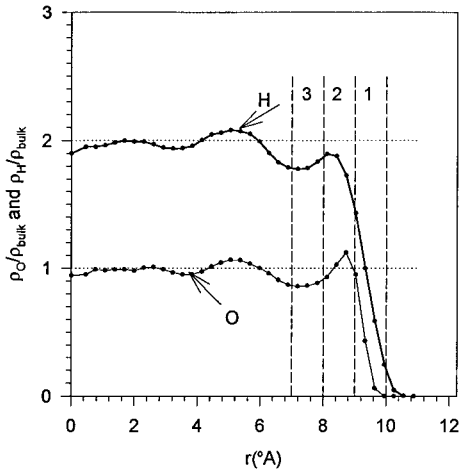

Figure 6. Density profile of oxygen and hydrogen atoms in the cylindrical pore. O; oxygen atoms; H; hydrogen atoms. The dotted lines correspond to the bulk values of oxygen and hydrogen atoms; the dashed lines indicate three layers near the wall.

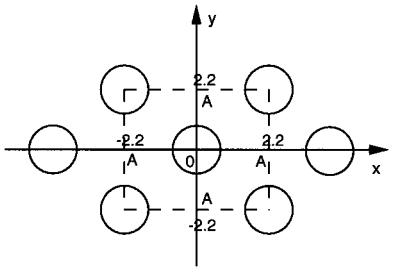

Figure 7. Wall atoms. A: the adsorption site.

than the bulk value of 2. This difference is attributed to the fact that, in the present work, ϵ_{WO} and ϵ_{WH} are much weaker than the energy depth of a 10-4-3 wall used in the work of Zhu and Robinson.[27] It is also observed that the hydrogen atoms can approach the wall more closely than the oxygen atoms. This happens because hydrogen atoms are relatively small and water molecules tend to orient with the hydrogen atoms toward the wall.

In order to demonstrate the detailed structures of water molecules near the wall, we select a wall atom on the surface of the pore together with its neighbors and then study the density distributions of water molecules in the three layers above this atom. This selection around a central atom (at $x = y = 0$) is depicted in Figure 7. In this case, each layer in the z direction has a width of 1 Å as indicated in Figure 6. The detailed concentrations of the oxygen and hydrogen atoms at the three layers around the central atom are shown in Figure 8. We observe that in the first layer both the hydrogen and the oxygen atoms locate preferentially at adsorption sites, which are denoted by the letter A in Figure 7. Due to the core repulsion the oxygen atoms will not stay on the top of the wall atom. The second layer corresponds to the first density peak near the wall. In this layer the oxygen atoms still prefer to locate at the adsorption sites, while the distribution of hydrogen atoms becomes less ordered. The third layer contains the first density valley near the wall. In this layer, the densities of both the hydrogen and oxygen atoms are higher on the top of the wall atoms than at the adsorption sites. This is due to the lack of atoms in the corresponding lower layers. The fact that water is unable to effectively "wet" the carbon wall has a significant effect on the dynamic behavior of water such as viscosity and velocity distributions.

It must be pointed out that one can extend the GENB method to noncubic, complex-geometry systems of two or three dimensions. For this purpose, one may define the parameters $a = D_x/D$, $b = D_y/D$, and $c = D_z/D$, where D_x, D_y, and D_z are the lengths of the cell in the three dimensions and D is a characteristic dimension. Hence, the magnitude of the distance between the positions of particles u and v and all of its images can be represented as follows:

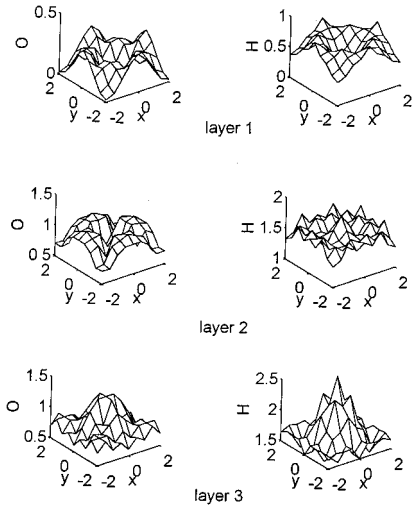

Figure 8. Structure of water molecules near a wall atom. The positions of the three layers are indicated in Figure 6.

$$dr = |\vec{r}(u) - \vec{r}(v) + D(a_l\vec{i} - b_m\vec{j} + c_n\vec{k})| \quad (32a)$$

where the vectors i, j, and k are the unit vectors in the three dimensions and the integers l, m, and n vary from minus infinity to plus infinity. Hence we may write for the distance dr

$$dr = D(a^2l^2 + b^2l^2 + c^2l^2)^{1/2}(1 + \beta)^{1/2} \quad (32b)$$

In this case, β is a function of a, b, c, l, m, n, $r(u)$, and $r(v)$ and, for a given geometry, a, b, and c are constants. One may follow the same procedure as in the previous sections and obtain the general expansion form for the energy function. The pertinent coefficients may be obtained by fitting the exact energy of a particular system by the least square method. This procedure can be easily adapted to complex two-dimensional systems, where $D_x = D_y$.

5. Conclusions

The general expansion method has been developed to calculate the long-range interactions due to the particles outside the minimum images, for three kinds of periodic systems. The derived formulas are valid, even if the charge neutrality condition is not satisfied. In this case the potential at a point should be interpreted as the relative potential, that is the difference between the real potential and a uniform background potential. We have presented the expansion coefficients for $\lambda \leq 2$ for 1PD and 2PD, and for $\lambda = 1$ for 3PD. It must be pointed out that the general expansion method is very versatile and may be further extended to complex systems, such as the central cell with different geometries, or particles with dipole−dipole interactions.

The neighbor-box technique is also used to improve the computational efficiency of long-range interactions. The trilinear element with 8 nodes and the complete quadratic element with 27 nodes are considered. Under the same conditions, the 27-node box is more accurate while the 8-node box is more efficient in computations. Larger box size leads to higher accuracy under the same node numbers. The combination of the general expansion method and the neighbor-box technique is the GENB method. If the total box number is optimized,

the GENB method renders the operation of long-range interactions proportional to $N^{3/2}$.

Acknowledgment. Partial support for this research was provided by grants from the NSF and LEQSF to Tulane University, for which the authors were thankful.

References and Notes

(1) Ewald, P. P. *Ann. Phys.* **1921**, *64*, 253.
(2) Adams, D. J.; McDonald, I. R. *J. Phys. C* **1974**, *7*, 2761.
(3) DeLeeuw, S. W.; Perram, J. W.; Smith, E. R. *Proc. R. Soc. London.* **1980**, *A373*, 27.
(4) Hansen, J. P. *Molecular-Dynamics Simulation of Statistical-Mechanical Systems*; Ciccotti, G., Hoover, W. G., Eds.; North-Holland: Amsterdam, 1986; p 89.
(5) Llano-Restrepo, M.; Chapman, W. G. *J. Chem. Phys.* **1994**, *100*, 8321.
(6) Natoli, V.; Ceperley, D. M. *J. Comput. Phys.* **1995**, *117*, 171.
(7) Caillol, J. M. *J. Chem. Phys.* **1994**, *101*, 6080.
(8) Perram, J. W.; Petersen, H. G.; DeLeeuw, S. W. *Mol. Phys.* **1988**, *65*, 875.
(9) York, Y.; Yang, W. *J. Chem. Phys.* **1994**, *101*, 3298.
(10) Luty, B. A.; Tironi, I. G.; Gunsteren, W. F. V. *J. Chem. Phys.* **1995**, *103*, 3014.
(11) Barker, J. A.; Watts, R. O. *Mol. Phys.* **1973**, *26*, 789.
(12) Watts, R. O. *Mol. Phys.* **1974**, *28*, 1069.
(13) Friedman, H. L. *Mol. Phys.* **1975**, *29*, 1533.
(14) Adams, D. J.; McDonald, I. R. *Mol. Phys.* **1976**, *32*, 931.
(15) Smith, P. E.; Gunsteren, W. F. V. *J. Chem. Phys.* **1994**, *100*, 3169.
(16) Lekner, J. *Physica A* **1991**, *176*, 485.
(17) Ladd, A. J. C. *Mol. Phys.* **1977**, *33*, 1039.
(18) Greengard, L. F. *The Rapid Evaluation of Potential Fields in Particle Systems*; The MIT Press: Cambridge, MA, 1988.
(19) Lambert, C. G.; Darden, T. A.; Board, J. A. J. *J. Comput. Phys.* **1996**, *126*, 274.
(20) Hockney, R. W.; Eastwood, J. W. *Computer Simulation Using Particles*; McGraw-Hill: New York, 1981.
(21) Dhatt, G.; Touzot, G.; Cantin, G. *The Finite Element Method Displayed*; John Wiley & Sons: New York, 1984.
(22) Bathe, K. J. *Finite Element Procedures in Engineering Analysis*; Prentice-Hall, Inc.: Englewood Cliffs, NJ, 1982.
(23) Lee, C. Y.; McCammon, J. A.; Rossky, P. J. *J. Chem. Phys.* **1984**, *80*, 4448.
(24) Christou, N. I.; Whitehouse, J. S.; Nicholson, D.; Parsonage, N. G. *Mol. Phys.* **1985**, *55*, 397.
(25) Spohr, E. *J. Phys. Chem.* **1989**, *93*, 6171.
(26) Raghavan, K.; Foster, K.; Motakabbir, K.; Berkowitz, M. *J. Chem. Phys.* **1991**, *94*, 2110.
(27) Zhu, S. B.; Robinson, G. W. *J. Chem. Phys.* **1991**, *94*, 1403.
(28) Rose, D. A.; Benjamin, I. *J. Chem. Phys.* **1993**, *98*, 2283.
(29) Lee, S. H.; Rossky, P. J. *J. Chem. Phys.* **1994**, *100*, 3334.
(30) Zhu, S. B.; Philpott, M. R. *J. Chem. Phys.* **1994**, *100*, 6961.
(31) Berendsen, H. J.; Grigera, J. R.; Straatsma, T. P. *J. Phys. Chem.* **1987**, *91*, 6269.
(32) Hoover, W. G. *Computational Statistical Mechanics.* Elsevier Science Publisher: New York, 1991.
(33) Gunsteren, W. F. V.; Berendsen, H. J. C. *Mol. Phys.* **1977**, *34*, 1311.
(34) Verlet, L. *Phys. Rev.* **1967**, *159*, 98.